Final version available at IoPScience : http://dx.doi.org/10.7567/JJAP.57.02BC03

Characterization of interfacial morphology of low temperature, low pressure Au-Au thermocompression bonding

M.S. Goorsky[1,4], K. Schjølberg-Henriksen[2], B. Beekley[1], T. Bai[1], K. Mani[1], P. Ambhore[1,4], A. Bajwa[1,4], N. Malik[3] and S.S. Iyer,[1,4]

[1]*Materials Science and Engineering, University of California, Los Angeles. 90095, USA*
[2]*SINTEF ICT, P.O. Box 314 Blindern, 0314 Oslo, Norway*
[3]*Centre for Materials Science and Nanotechnology, University of Oslo, 0316 Oslo, Norway*
[4]*Center for Heterogeneous Integration and Performance Scaling, University of California, Los Angeles. 90095, USA*

[*]E-mail: goorsky@seas.ucla.edu

Au-Au thermocompression bonding is a versatile technique of high interest for a variety of applications. We have investigated Au-Au bonding using sputter deposited Au films under conditions of low temperature (150 °C – 250 °C) and low bonding pressure (~ 3 MPa) for short times (15 minutes). The combination of low temperature and short times is important for applications involving both hermetic sealing and packaging scaling. The initial surface roughness of the Au film was in the 3-5 nm range with peak-to-valley heights of 20-30 nm and a lateral correlation length of ~ 400 nm. For samples bonded at 150 °C, the void morphology at the bonded interface was related to the initial surface roughness. The void morphology was different when bonding at the higher temperatures: the void length (along the bonded interface) decreased significantly but the void height (perpendicular to the interface) increased. These results can be understood in terms of a combination of increased surface Au diffusivity and decreased yield stress and elastic modulus with increased bonding temperature.

1. Introduction

Thermocompression bonding of Au surfaces is an important technology for advanced circuits and systems. Applications include, but are not limited to, hermetically sealed MEMS sensors[1], CCD / CMOS cameras[2], wafer-scale integration, and low pitch-dimension packaging scaling[3]. While both Cu[4] and Al[5] are also used for metal thermocompression bonding, Au is especially attractive for thermocompression bonding because it does not form a native oxide, it can be deposited by a wide variety of techniques with good pitch control and resolution, it is a biocompatible material, and it can be used in harsh environments. Several prior studies of Au thermocompression bonding[6-9] have focused on relatively higher bonding temperatures (260 °C and higher) and longer times. Recently, several efforts to lower the temperature requirements for Au-Au thermocompression bonding have involved more complicated processes. Ar ion surface activation of low roughness (0.34 nm root mean square (r.m.s.) roughness) Au films bonded at room temperature to a smooth glass wafer[10] and the use of nanolayer thickness Au films with very low surface roughness[11] have resulted in successful bonding at room temperature. More recently,[12] this approach was developed using 50 nm Au films. For these thin films, the surface roughness is sufficiently low (< 1 nm r.m.s. roughness) that low force, low temperature bonding is feasible. By utilizing a subsequent Ar rf radio plasma surface treatment, organic contaminants on the surface were removed prior to binding and high mechanical strength bonds resulted. Smooth surfaces[13] for bonding can also be produced by a mechanical pressing technique to produce < 1 nm r.m.s. roughness from Ag layers with an initial roughness of 13 nm by using high applied force (> 500 MPa) with a smooth surface (Si wafer) at room temperature. Another approach [14-15] involved an initially rough (16 nm) Au surface that achieved < 1 nm roughness which was replicated from an atomically smooth master substrate by a lift-off process using a sacrificial layer. Further, compressible nanoporous Au films have been shown to reduce the bonding temperature to ~ 200 °C through de-alloying deposited Au-Sn alloy layers[16], through de-alloying Ag-Au films[17] and using an intermediate nanoporous printed Ag layer[18].

Based on these studies, it appears that both the initial surface roughness of the Au film and – at least qualitatively – the impact of the change in Au mechanical properties (through nanoporous material formation, for example) are of significance for the film bondability. The bonding of very flat surfaces is fairly well understood, but there is somewhat less information

about the interface morphology of Au-bonded interfaces with intermediate roughness values. Information from Cu-Cu bonded interfaces, however, can provide some insight into the general issues. It should be noted that Cu surfaces typically include a copper oxide surface layer – which may or may not be continuous; fortunately, Au surfaces do not contain oxide layers. In addition, the designation of a 'low' or 'high' temperature is dependent on the metal; therefore, it is useful to also note the homologous temperature (T_H), or the fraction of the annealing temperature to the melting temperature. For low temperature bonding of Cu-Cu structures[19] (175 °C; T_H = 0.33), the surface roughness was found to play a key role in determining the minimum temperature at which bonding occurred as well as the quality of the bonded interface, although a detailed assessment of the interface void morphology was not provided. As noted above for the Au-based thermocompression studies, smoother surfaces had been shown to promote bonding at lower temperatures and reduce the presence of interfacial voids. Another recent study[20] of metal-metal bonding noted that, for Cu-Cu bonding, initially rough surfaces (r.m.s. roughness = 33 nm) led to the formation of large (μm-scale) voids after thermocompression bonding [at 400 °C (T_H = 0.5), 2-3 MPa, one hour] but very smooth surfaces (0.2 nm r.m.s. roughness) produced, after the same thermocompression bonding, only very small voids (few nm-scale) with about a two order of magnitude reduction of the interfacial void volume. That study[20] also showed an example of Au–Au thermocompression bonding with initial surface roughness of 2.7 nm (approximately 1 order of magnitude difference from both the very low and very high roughness of the Cu surfaces) and subject to thermocompression bonding at 500 °C (TH = 0.58, otherwise same conditions as above). After the bonding step, very large voids (~μm wide along the interface and ~0.2 μm across the interface) extended over several grains. This "intermediate" surface roughness is especially interesting as it is typical of Au deposited surfaces that have been subject to only modest chemical–mechanical polishing[21]. The bond interface morphology is expected to be determined by the diffusion of Au atoms during bonding step as well as the deformation of the interface due to the applied compression during bonding. Surface diffusion of Au has been studied extensively. One study[22] and references therein show that surface diffusion is significantly higher than bulk diffusion in our experimental temperature range but the values from different references vary significantly. In general, the references indicate that the surface diffusion at 250 °C is 10–

100 times the value at 150 °C and thus it might be expected that different factors dominate the bonding morphology. The mechanical properties of metals are also temperature dependent. The yield stress for Au[23] is reported to decrease somewhat linearly as a function of increasing temperature and decreases from 114 MPa at 150 °C to 102 MPa at 250 °C—or approximately a 10% decrease. The Young's modulus also shows a similar dependence[24] with approximately a 10% decrease over this range. The aim of the present research, therefore, is to study the interface morphology of Au–Au thermocompression bonded interfaces, realized with sputter deposited Au films with intermediate surface roughness in a lower temperature bonding regime (150–250 °C, TH = 0.32–0.39). In particular, the role of the initial surface morphology and roughness on the formation of interfacial voids is addressed, as is the difference in the void characteristics after bonding over this low temperature range. A prior conference proceedings extended abstract[25] only touched on these issues; this work reports much more extensive data and analysis.

2. Experimental methods

The thermocompression bonded structures used here were described in an earlier study[26]. In brief, three wafer laminates were manufactured by Au-Au thermocompression bonding. A top wafer with silicon membranes was bonded to a flat silicon bottom wafer. Both wafers had a 1.2 µm thick Au bond frame layer which was sputter deposited on top of a sputter deposited 0.4 µm thick TiW adhesion layer. The Au bond frames had an inner dimension of 3.34 × 3.34 mm^2 and a frame width of 200 µm. The surface roughness of the Au film was measured by AFM in two 40 × 40 μm^2 regions outside the bonding area. Further, the texture of the Au film was investigated by x-ray diffraction.

The laminates were bonded in an SB6e (Suss MicroTec) wafer applying a tool pressure of 2266 mbar at bonding temperatures ranging from 150–250 °C for 15 minutes. The applied tool pressure corresponded to an average bond pressure of 10 MPa. The estimated bond pressure on each frame depends on the frame area and the amount of unbonded area surrounding the frame. The estimated bond pressure was 3 MPa on the frames of 200 µm width. After bonding, the hermetic yield, the dicing yield, and the bond strength were measured[19]. A top view of the selected chip design is shown in Fig. 1.

The microstructure at and around the bonded interface was studied using a Nova 600 focused ion beam (FIB) scanning electron microscope (SEM). First, the bonded samples were cross-sectionally diced then mounted in the FIB/SEM for cross-sectional milling. The FIB cut was begun at the start of the Au-Au bonded region and, once the cross-section surface was exposed, the surface was cleaned using the FIB at a lower current (0.5 nA). Subsequent cleaning cuts were taken with a depth of 0.05 – 0.6 μm steps and images were taken to create a three-dimensional (3D) reconstruction of the interface[27-29]. For each bonded interface, void dimensions were characterized over 200 μm of interface length to generate statistically useful information. A similar process was used to produce plan-view images and 3D reconstructions, but the initial cut was taken at the Si wafer parallel to the bonding interface and the cleaning slices were milled from the Si into the Au and across the interface. Figure 2 shows a schematic of the initial cuts and subsequent milling for the 3D FIB reconstructions.

Transmission electron microscopy samples were also produced from the bonded structures (FEI Titan 300). Voids at the Au-Au bonding interface, observed in the SEM images, were analyzed with respect to void length (cross section), diameter (plan view), and height (cross section). Atomic force microscopy images were obtained (Quesant Q-scope) with areas typically 40 μm x 40 μm and 30 μm line scans. X-ray diffraction patterns were produced using a Jordan Valley (now Bruker) D1 with Cu kα radiation, an incident beam optic to produce a parallel beam and scattered beam slits (~ 0.1°).

3. Results and discussion

3.1 Non-bonded wafers

The x-ray diffraction pattern from the as-deposited Au film is shown in Fig. 3. The Figure shows the same data plotted on a linear intensity scale and a logarithmic intensity scale. From the linear scale, the sputtered Au exhibited strong (111) texturing as only (111) and (222) reflections were clearly observed. From the log intensity scale, however, other weak Au peaks ((200), (220), (311)) were observed as well as TiW peaks. The diffraction pattern of the annealed (250 °C for 15 minutes; similar to the bonding conditions but without the compression) was indistinguishable from that shown in Fig. 3. The 40 μm x 40 μm atomic force microscopy measurements in Fig. 4 shows that the as-deposited Au surfaces were of

the ‘intermediate’ roughness range – with roughness values of 4.5 – 5.5 nm. Analysis of line scans indicated that the average height of the peaks was about 17 nm with the maximum asperities ~ 35 nm. The average period between peaks was approximately 400 nm over a 30 μm scan. Figure 5 shows AFM line scans from Au surfaces before and after annealing. The scans for each wafer were taken in the same position. Figure 5(a) shows the difference in the line scan for a wafer prior to annealing (5.1 ± 0.2 nm r.m.s.) and after annealing at 150 °C (4.9 ± 0.2 nm r.m.s.); there was no measurable change in the roughness. Figure 5(b) shows the difference in the line scan for a wafer prior to annealing (4.9 ± 0.2 nm r.m.s.) and after annealing at 250 °C (3.2 ± 0.2 nm r.m.s.); there was a significant change in the roughness after the higher temperature step.

3.2 Thermocompression bonded interfaces

The cross-sectional SEM images prepared using the FIB show the cross-section shape, size and distribution of voids along the Au-Au bonding interface. SEM cross section interfaces from samples bonded at 150 °C and 250 °C are shown in Figure 6. The samples bonded at 150 °C show voids with long extension along the interface (the void length) with little extension across the interface (void height), In contrast, the samples bonded at 250 °C show discrete voids interspaced with well bonded regions. For the samples bonded at 250 °C, the voids are much more equiaxed, with much shorter void lengths than the sample bonded at 150 °C but with somewhat greater void heights. The grain sizes in all samples are the same – the average grain size is 0.4 μm with a 0.15 μm standard deviation.

Cross section images only provide a one-dimensional view of the void morphology. Sequential FIB cuts through a cross section and sequential cuts along the interface to show plan view images provide a better assessment of the void morphology. Figure 7 shows a reconstruction of the bonded interface of a chip bonded at 200 °C. Figure 7(a) shows a plan view image from 0.12 μm above the interface, Fig, 7(b) shows the plan view void morphology across the interface and Fig, 7(c) is from 0.15 μm below the interface. In all cases, the void morphology is varied; while some roughly equiaxed voids exist, many of the voids are elongated or show branching. In Fig. 7(a) and 7(b), the box highlights a branched triangular void. Because the same feature is present at both depths, this void extends from

above the interface to the interface. However, the feature is absent below the interface. Similarly, the circled region shows a pair of voids that extend from below the interface to the interface. There are also some voids which extend across the interface for the samples annealed at 200 °C and 250 °C (e.g., Fig, 6(b) shows this in cross-section). Additionally, the contrast in the images reveals the individual grains and shows that the voids are present at the grain boundaries – in these images, no voids were observed in an intragranular region. Figure 8 shows the plan view void morphology at the interface bonded at 150 °C. The Figure shows the presence of large void networks, covering 50% of the bonded interface area.

The transmission electron microscopy results provide further insight into the nature of the bonded interface. Figure 9(a) shows a bright field image from the sample bonded at 250 °C. The dark line contrast features near the interface are related to the plastic deformation there (the samples bonded at 150 °C did not exhibit this type of deformation). Selected area diffraction from the grains adjacent to the void show that both are (111) grains aligned perpendicular to the interface, consistent with the x-ray diffraction measurements which show the high extent of (111) texturing. The interface at that location includes a void which extends only one side of the interface. The void that exists between these two grains is shown in high resolution (Figure 8(b)) and the facetted nature of the void is delineated in the figure.

Figure 10 shows the void dimensions for the different annealing steps based on the analysis of the cross section (length and height) and plan view (diameter) SEM images. Note that the void length (diameter) decreases significantly when the bonding temperature was 200 °C compared to 150 °C, and decreases slightly more for the 250 °C bond temperature. The void height (perpendicular to the interface) shows an opposite trend; the void height increases the most when considering the bond temperature of 200 °C compared to 150 °C and increases, but less so, comparing bonding at 250 °C versus 200 °C.

3.3 Discussion

The characterization of the non-bonded wafers led to some key points. First, the diffraction measurements showed the Au films are very highly (111) oriented and that the diffraction pattern did not change with annealing. There were no metallurgical interactions within the layers in the film – either at the Au-TiW or TiW-Si interfaces. The peak widths also did not change, indicating that there was not significant grain growth perpendicular to the interface.

This was also shown through the plan view SEM measurements of the interface. While previous reports[21] indicated that there was a one to two order magnitude different in Au surface diffusion at 150 °C and 250 °C, the values in the literature at a given temperature varied by several orders of magnitude such that, based on those values, one could predict that there would a) not be noticeable diffusion on either annealed surface or that b) both annealed surfaces would show extensive surface diffusion. These measurements here show (Fig. 5) negligible diffusion on the surface after 150 °C annealing but the surface annealed at 250 °C shows significant surface diffusion. Of course, these surfaces are not subjected to the compression force as is the case during thermocompression bonding; surface diffusion during bonding is a subject of current study but these results do indicate that the kinetics of atomic motion is significantly different at 150 °C and 250 °C.

The results obtained in the current study of the bonded structures support and explain the earlier results reported on these samples. It was found that the dicing yield was 100% the samples bonded at all temperatures, showing that the areas that did bond provided a seal which was strong enough to withstand the force exerted by the wafer dicer[29]. The results in the current study show that for all samples, at least 50% of the frame area appears to be bonded. This bonded area is likely to account for the high dicing yield.

From the earlier studies, there was a large increase in hermetic yield when increasing the bonding temperature from 150 °C to 200 °C. The hermetic yield of the sample types was below 11% for samples bonded at 150 °C, 55-61% for samples bonded at 200 °C, and 69% for samples bonded at 250 °C[19] This observation is explained by the current results on void height and length. As seen in Fig. 8, at 150 °C, bonding had occurred in isolated areas which were surrounded by a network of voids. As a result, these samples were not hermetically sealed. However, it is speculated that in 4 – 11% of the samples bonded at 150 °C, a continuous bonded area was present along the entire bond frame, rendering some samples hermetically sealed. In most of the samples bonded at 200 and 250 °C, there was a continuous bonded area along the entire bond frame, giving a high hermetic yield in addition to the high mechanical strength.

More fundamental results can also be gleaned from the analysis of the void formation. For the samples bonded at 150 °C, the average void width of 480 nm is comparable to the pre-bonded correlation length as determined by the AFM line scan. Likewise, the void

heights (40-50 nm) are also consistent with the asperity height (~30 nm for each face or a maximum of 60 nm if asperities touch and there is not significant deformation or diffusion). The AFM measurement before and after annealing at 150 °C (Fig. 5a) indicates there is negligible diffusion and this is also consistent with the observed void dimensions. Greater surface diffusion would be expected to fill in the valleys in the surface and the lack of significant deformation from the TEM for this sample indicates that the yield strength and Young's modulus at 150 °C are sufficiently high that the void morphology after bonding at 150 °C is primarily related to the pre-bonded surface roughness. This suggests that for a T_H of ~ 0.3, stress-induced diffusion and void morphology changes (i.e., creep) are not significant.

Thermocompression bonding at 200 °C and 250 °C show a very different void behavior than bonding at 150 °C. Smaller in-plane void dimensions and larger out-of-plane dimensions point to different kinetics in that diffusion and deformation play a larger role. The increase in surface diffusion supports the reduction in the void width as Au atoms at the asperity tips can diffuse to the open regions at the interface. Also, combined with the TEM and SEM data that shows that the voids form at the boundaries between two grains, the enhanced diffusion promotes the movement of Au atoms from the grain boundary interface to the bond interface. The smaller voids observed at these temperatures tend to exist on only one side of the interface whereas the larger voids extend across both sides of the bonded interface. The TEM images at these temperatures also show significant plastic deformation. We conclude that the reported decrease in yield stress with increasing temperature is related to the reduced void length at higher temperatures as well as the presence of the plastic deformation near the interface. Future work includes comparing these results with samples bonded at similar temperatures but at significantly higher (> 5x) bonding pressure to better ascertain the relative roles of surface diffusion, bonding temperature, and bonding pressure for these structures with intermediate (few nm r.m.s. roughness) surface roughness values.

4. Conclusions

Au-Au thermocompression bonding using sputter deposited Au films under conditions of low temperature (150 °C – 250 °C) and low bonding pressure (~ 3 MPa) for short times (15 minutes) was investigated. The initial surface roughness of the Au film was in the 3-5 nm

range with peak-to-valley heights of 20-30 nm and a lateral correlation length of ~ 400 nm. For samples bonded at 150 °C, the void morphology at the bonded interface was related to the initial surface roughness. The void morphology was different when bonding at the higher temperatures: the interfacial length or diameter of the voids decreased significantly but the height of the voids across the interface increased. These results can be understood in terms of a combination of increased surface Au diffusivity and decreased yield stress and elastic modulus with increased bonding temperature. The results indicate that strong bonds can be realized at 150 °C, while hermetic seals require a bond temperature of 200 °C when using sputter deposited Au films with intermediate values of initial surface roughness.

Acknowledgments

The Defense Advanced Research Projects Agency (DARPA) through ONR grant N00014-16-1-263 and the UCLA CHIPS Consortium supported this work. The authors also gratefully acknowledge financial support from the Research Council of Norway, contract No 247781.

References

1) R. Fraux and J.Baron, 3D Packaging **21,** 24 (2011).

2) M. Goto, K. Hagiwara, Y. Iguchi, H. Ohtake, T. Saraya, M. Kobayashi, E. Higurashi, H. Toshiyoshi, T. Hiramoto, IEEE Trans. Electron Devices, **62,** 11 3530 (2015).

3) K. Schjølberg-Henriksen, J. Gjessing, K. A. H. Bakke, S. Hadzialic, D. T. Wang, Proc. SPIE, 10108, Silicon Photonics XII, 101080P (2017).

4) L. Di Cioccio, F. Baudin, P. Gergaud, V. Delaye, P.-H. Jouneau, F. Rieutord, and T. Signamarcheix, ECS Trans. 64 [5], 339 (2014).

5) N. Malik, K. Schjølberg-Henriksen, E. U Poppe, M. Taklo, and T. G. Finstad, J. Micromech. Microeng. **25** 1 (2015).

6) C. H. Tsau, S. M. Spearing, and M. A. Schmidt, J. Microelectromech. Syst., **13,** 6 (2004).

7) M. Taklo, P Storås, K Schjølberg-Henriksen, H. Hasting and H. Jakobsen, J. Micromech. Microeng. **14,** 884 (2004).

8) D. Xu, E. Jing , B. Xiong, and Y. Wang, IEEE Trans Adv. Pack. **33** 904 (2010).

9) H.R. Tofteberg, K. Schjølberg-Henriksen, E.J. Fasting, A.S. Moen, M.M.V. Taklo, C.J. Simensen, J. Micromech. Microeng. Vol 24, 084002 (2014).

10) K. Okumura, E. Higurashi, T. Suga and K. Hagiwara, 4th IEEE International Workshop on Low Temperature Bonding for 3D Integration (LTB-3D) 2014, p.26

11) T. Shimatsu, M. Uomoto, K. Oba, and Y. Furukata, 3rd IEEE International Workshop on Low Temperature Bonding for 3D Integration (LTB-3D), 2012, p.103

12) E. Higurashi, K. Okumura, Y. Kunimune, T. Sugua, and K. Hagiwara, IEICE Trans. Electron, **100–C,** 156 (2017).

13) V. Logeeswaran, M-L. Chan, Y. Bayam, M. Saif Islam, D. Horsley, X. Li, W. Wu, S.Y. Wang, R.S. Williams, Appl. Phys. A **87,** 187 (2007)

14) Y. Kurashima, A. Maeda, and H. Takagi, Microelectronic Engineering **129,** 1 (2014)

15) Y. Kurashima, A. Maeda, J. Lu. L. Zhang, H. Takagi, Microelectronic Engineering **119** , 48 (2014).

16) W-S Wang, Y-C Lin, T. Gessner, and M. Esashi, Japanese J. Appl. Phys. **54**, 030215 (2015).

17) H. Oppermann and L. Dietrich, Microelectronics Reliability, **52**, 356 (2012).

18) M. Wiemer, F. Roscher, T. Seifert, K. Vogel, T. Ogashiwa and T. Gessner, ECS Transactions, **75,** 299 (2016).

19) B. Rebhan and K. Hingerl, J. Appl. Phys. **118**, 135301 (2015).

20) P. Gondcharton, B. Imbert, L. Benaissa, and M. Verdier, ECS J. Sol. St. Sci. Technol. **4,** 77 (2015).

21) A. Bajwa, S. Jangam, S. Pal, N. Marathe, T. Bai, T. Fukushima, M. Goorsky, S.S. Iyer, IEEE 67th Electronic Components and Technology Conference, 2017, p. 1276

22) H. Göbel and P. von Blanckenhagen, Surface Science **331-333,** 885 (1995).

23) M. Poniatowski and M. Clasing, Gold Bull., **5,** 341 (1972).

24) S. Collard, Ph.D. Thesis, Rice U. (1991).

25) M.S. Goorsky, K. Schjølberg-Henriksen, B. Beekley, N. Marathe, K. Mani, A. Bajwa, and S.S. Iyer, 5th International Workshop on Low Temperature Bonding for 3D Integration (LTB-3D), 2017 p. 42

26) N. Malik, H. R. Tofteberg, E. Poppe, T. G. Finstad and K. Schjølberg-Henriksen, ECS J. Solid State Sci. Technol. 4, 236 (2015).

27) T. Sakamoto, Z. Cheng, M. Takahashi, M. Owari, and Y. Nihei, Jpn. J. Appl. Phys. 37, 2051 (1998).

28) B. J. Inkson, M. Mulvihill, and G. Möbus, Scr. Mater. 45, 753 (2001).

29) L. Holzer, F. Indutnyi, P. Gasser, B. Münch, and M. Wegmann, J. Microsc. 216, 84 (2004).

Figure Captions

Fig. 1. Top view of the bonded chip types layout. The frame is 200 µm wide, with rounded corners.

Fig. 2. Cross sectional drawing of the bonded interface, with the red dashed boxes showing the location of the initial regular cross section cuts and the direction of cleaning slices for the cross-section and plan-view images, respectively.

Fig. 3. X-ray diffraction pattern from the as-deposited Au film. Linear intensity scale (dashed line) and logarithmic intensity scale (solid line).

Fig.4. Atomic force microscopy measurement of the as-deposited Au surface revealed a surface roughness of 4.5 – 5.5 nm.

Fig. 5. AFM line scans from unbonded Au surfaces before and after annealing. a): annealing at 150 °C; b): annealing at 250 °C.

Fig. 6. SEM cross-section interfaces from samples bonded at a)150 °C and b) 250 °C.

Fig. 7. SEM sequential plan view images of the interface bonded at 200 °C. a) 0.12 µm above the interface. b) at the interface. c) 0.15 µm below the interface. The box (a and b) shows a branched, triangular void present above and at the interface. The circle shows a pair of voids present below and at the interface (b and c).

Fig. 8. SEM plan view of the interface bonded at 150 °C.

Fig. 9. a) TEM bright field image of the sample bonded at 250 °C . b) Higher magnification of the void in a), showing the faceted nature of the void.

Fig. 10. Average void length (squares), void diameter (circles) and void height (triangles)

for samples bonded at 150, 200, and 250 °C.

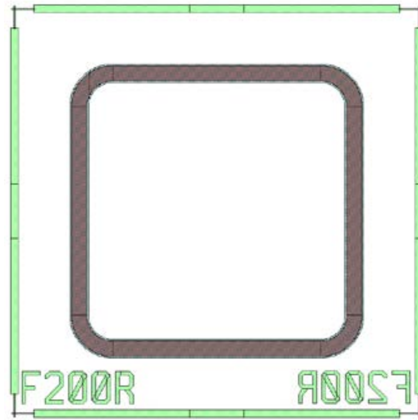

Figure 1 (Color online)

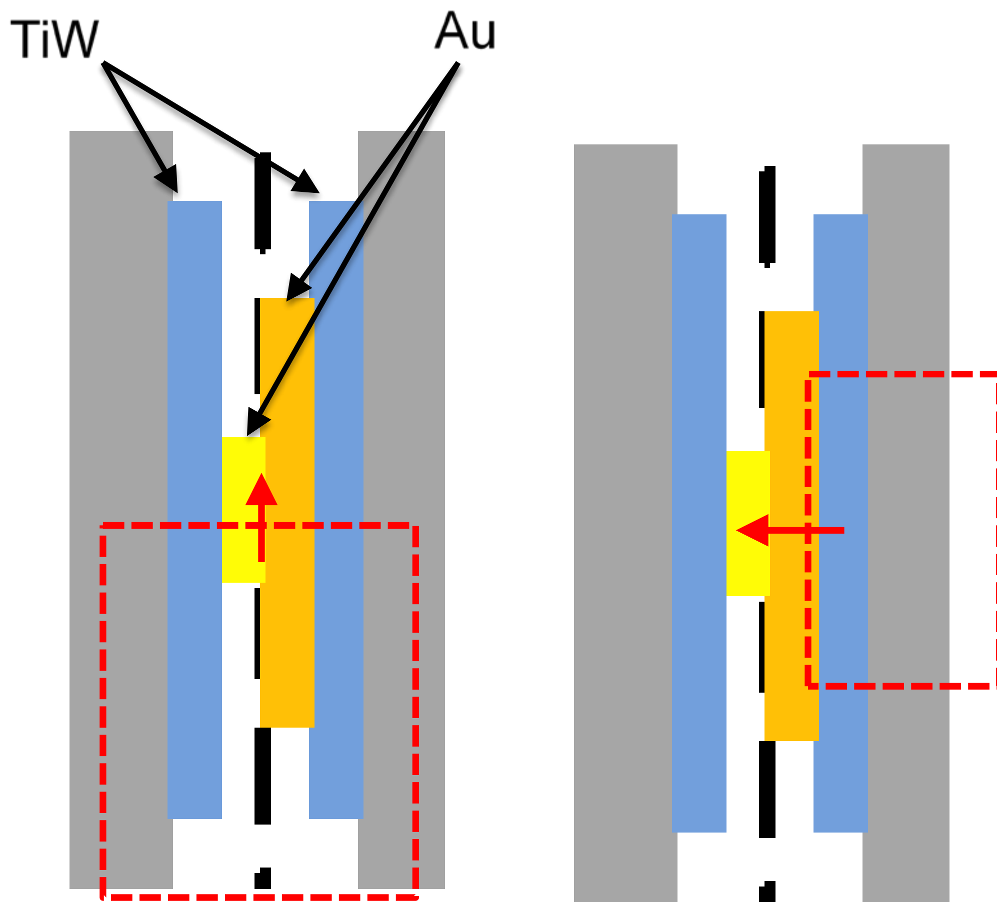

Figure 2

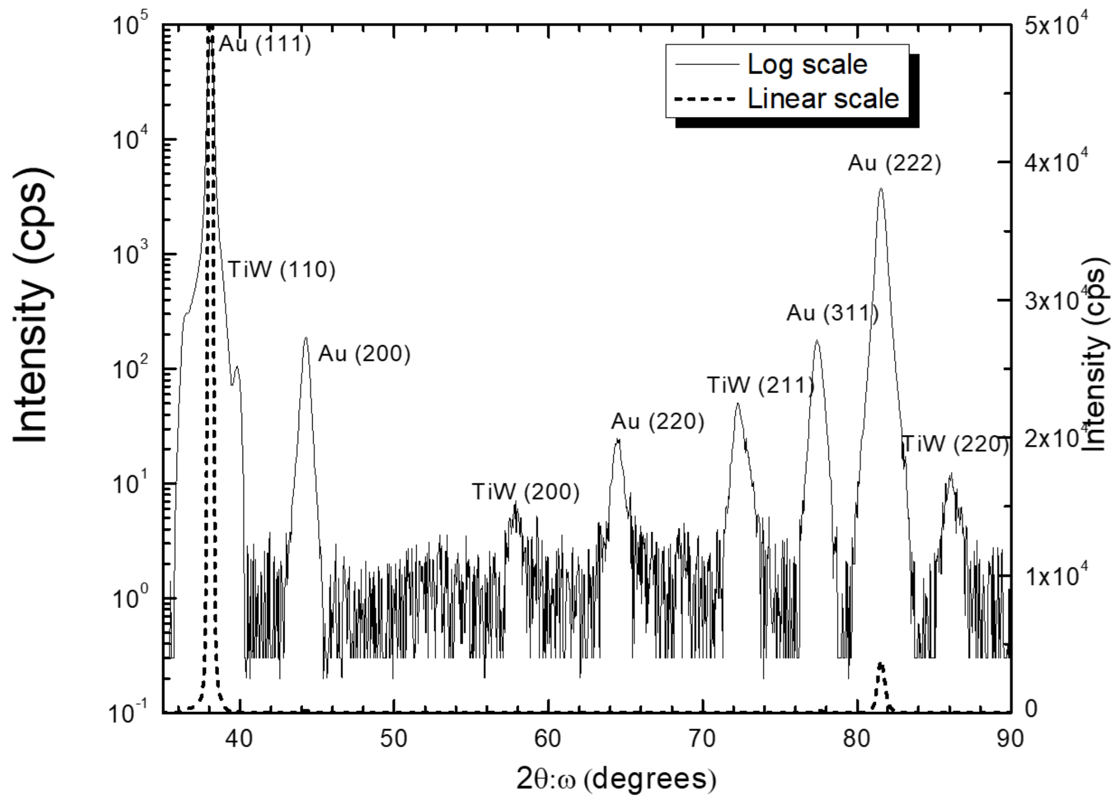

Figure 3

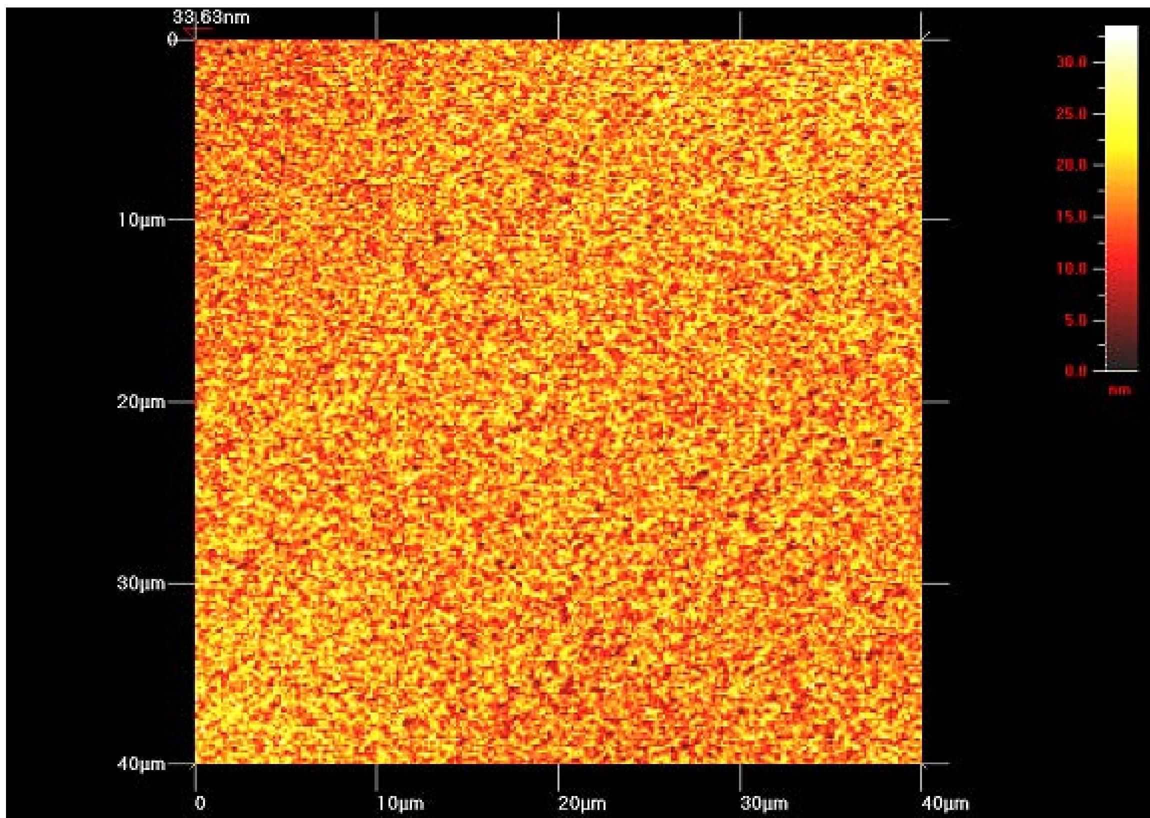

Figure 4

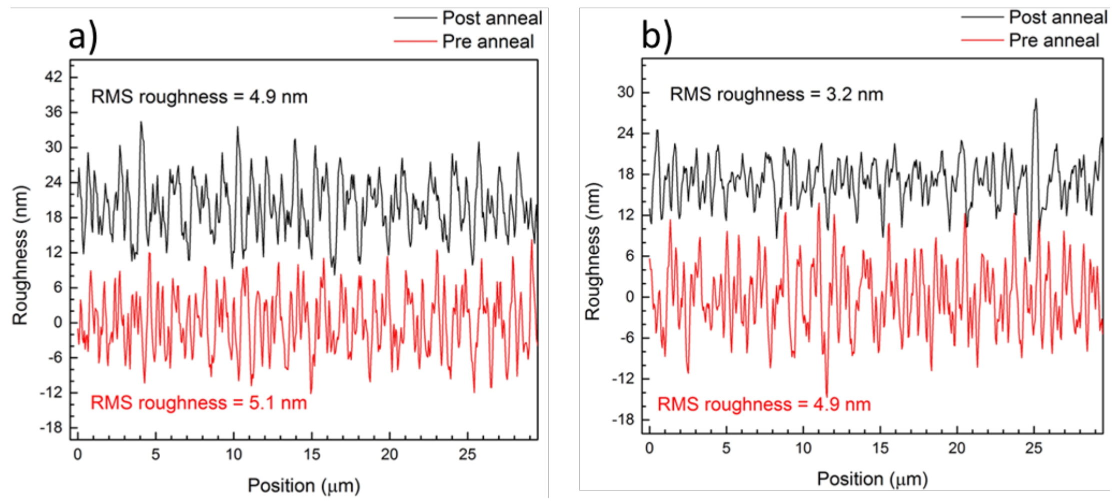

Figure 5

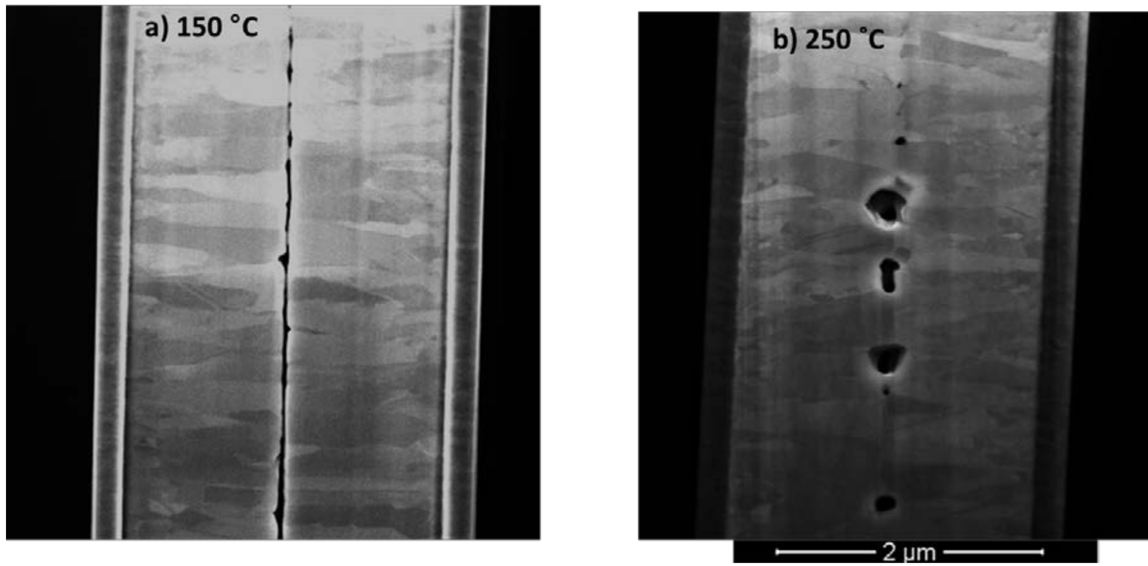

Figure 6

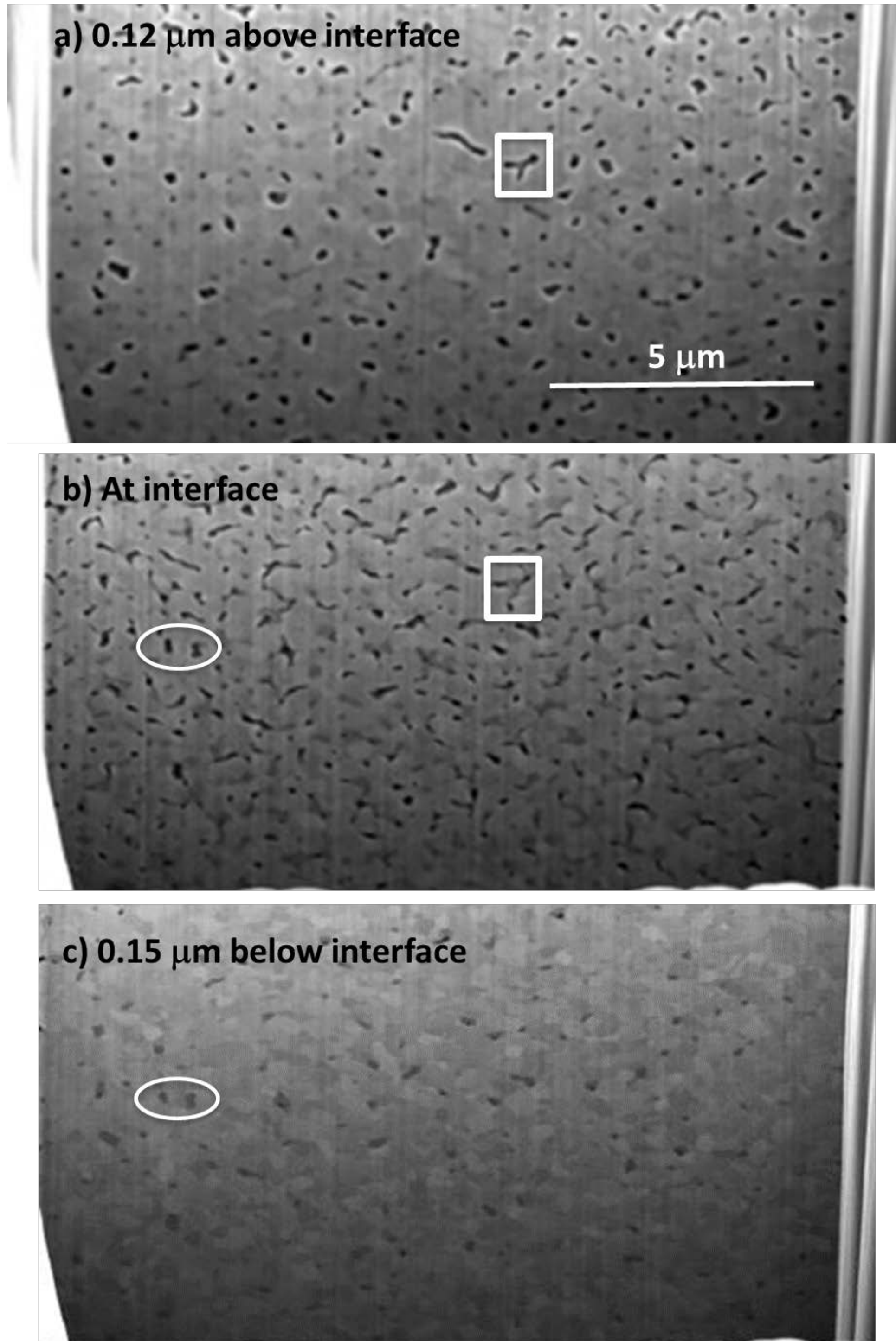

Figure 7

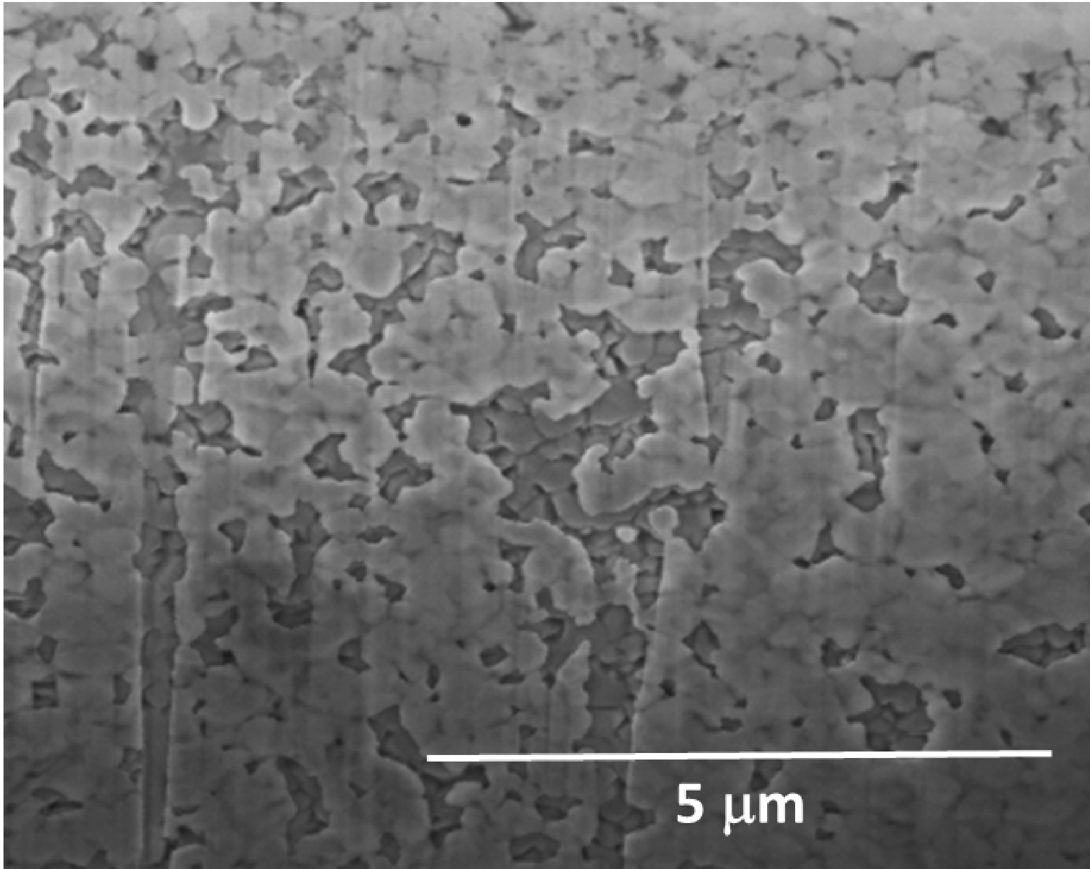

Figure 8

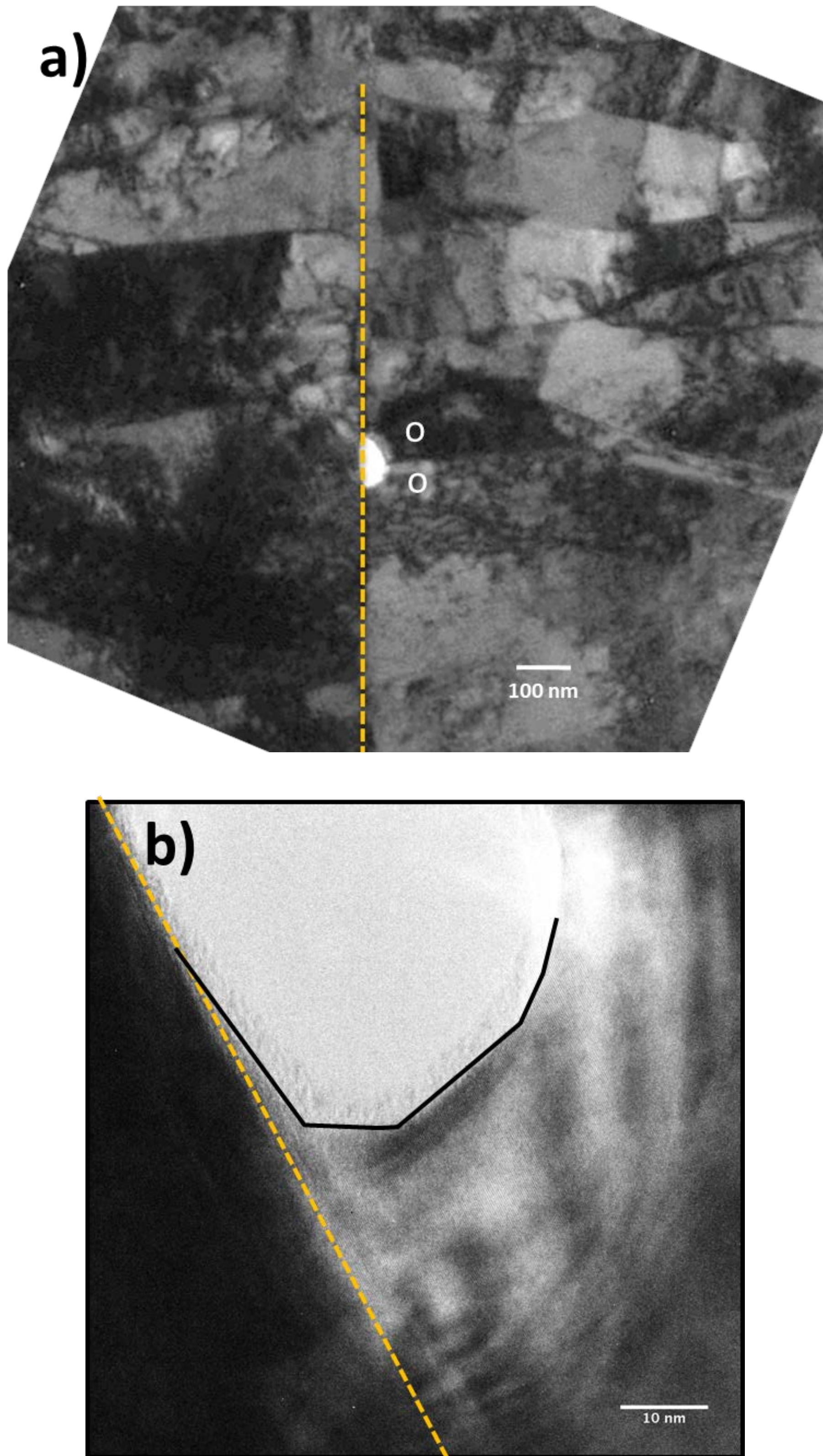

Figure 9

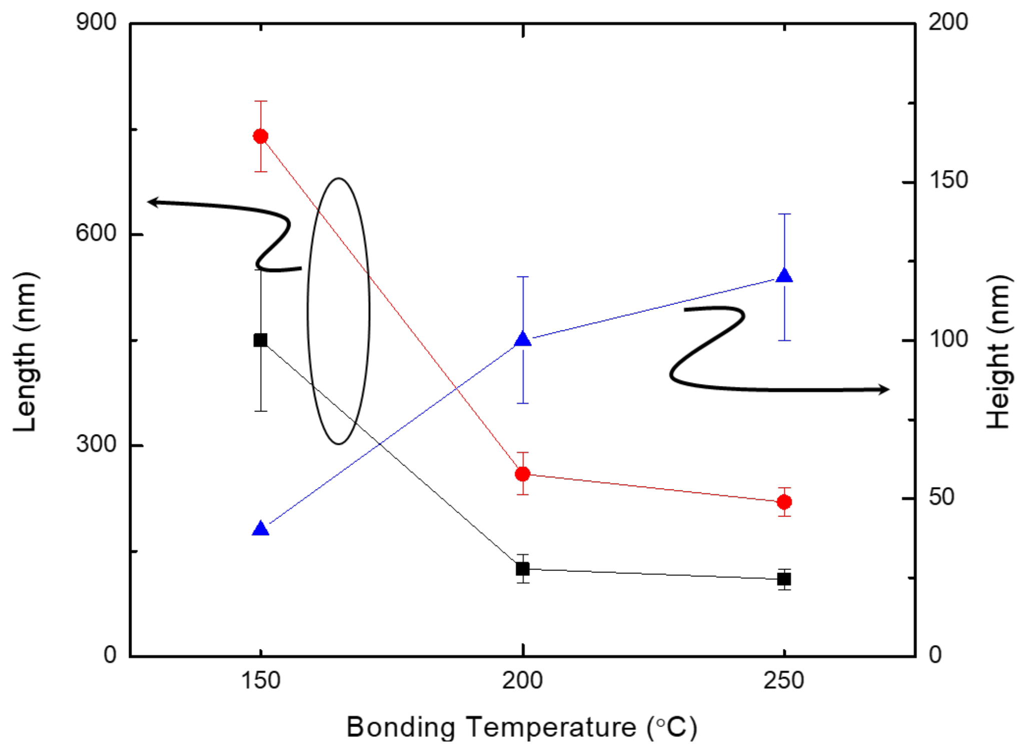

Figure 10